View Article Online / Journal Homepage / Table of Contents for this issue
Dynamic Article Links

PCCP

Cite this: *Phys. Chem. Chem. Phys.*, 2012, **14**, 16088–16095

www.rsc.org/pccp

PAPER

Composition of the outermost layer and concentration depth profiles of ammonium nitrate ionic liquid surfaces†

Christiaan Ridings,[a] Gregory G. Warr[b] and Gunther G. Andersson*[a]

Received 30th August 2012, Accepted 11th October 2012
DOI: 10.1039/c2cp43035e

Differences in the surface structure of protic ionic liquids (ILs) with three different cations and a common anion; ethyl-, propyl- and 2-hydroxyethyl- (or ethanol-) ammonium nitrate (EAN, PAN and EtAN, respectively) have been observed by neutral impact collision ion scattering spectroscopy (NICISS) and metastable induced electron spectroscopy/ultraviolet photoelectron spectroscopy (MIES/UPS). NICISS is used to determine the concentration depth profiles of the elements in each IL and it reveals an enrichment of cation alkyl chains of PAN and EtAN in the outermost layer compared to EAN, and a corresponding depletion of nitrate from the outermost layer of the EtAN surface. MIES probes the molecular orbitals of only the species in the outermost layer of a sample and confirms that, while both the anion and the cation are present to some degree at the surface of all three ILs, the cation is enriched to a greater extent at the surface of PAN and EtAN compared to EAN.

Published on 12 October 2012. Downloaded by Michigan State University on 19/01/2016 06:14:23.

1. Introduction

Ionic liquids (ILs) have been a subject of interest in many applications[1] such as solar cells,[2,3] solvents,[4] catalysis[5] and gas capture media.[6,7] Much of this attention is due to the vast range of possible cation–anion combinations which result in a large degree of freedom in tailoring the physical properties of the liquid.[4] Investigations into the surface structure of ILs play a key role in understanding surface physical properties such as surface potential and surface tension while also contributing to the fundamental understanding of processes occurring at the liquid/vapour interface. The IL/vapour interface has been studied using a wide variety of techniques such as the non-linear optical (NLO) methods,[8–10] X-ray reflectivity,[11–13] direct recoil spectroscopy (DRS),[14] X-ray photoelectron spectroscopy (XPS),[15–17] neutral impact collision ion scattering spectroscopy (NICISS)[18–20] and metastable induced electron spectroscopy/ultra-violet photoelectron spectroscopy (MIES/UPS).[21–23] These studies have all provided significant progress in understanding the surface structure of ILs, but the vast majority focus solely on aprotic ILs. Protic ionic liquids are made by the process of transferring a proton from a Brønsted acid to a Brønsted base[13] thus resulting in a high-degree of hydrogen bonding between the cation and the anion. Wakeham *et al*. have investigated the surface of ethylammonium nitrate (EAN), propylammonium nitrate (PAN) and ethylammonium formate (EAF) using X-ray reflectivity.[13] Their results indicate that there is a structure existing at the surface that extends to the bulk sponge-like morphology for 38 Å and 44 Å for EAN and PAN, respectively, and that this surface ordering is more pronounced in the case of PAN. This ordering is suggested to be due to the layering of polar and non-polar domains where the increased solvophobicity[24] (owing to the greater cation alkyl chain length) in PAN contributes to the increased definition of these layers, which can be seen in other results.[25,26] Furthermore the results by Wakeham *et al*. show a region of low density in the top several Å which is attributed to the formation of $C_8A_7^+$ (where C is the cation and A is the anion) aggregates at the surface. These clusters were originally observed by Kennedy and Drummond for a range of protic ILs and found to be independent of cation alkyl chain length.[25] Ludwig performed static quantum chemical calculations and determined that the $C_8A_7^+$ cluster is the most stable of the $C_nA_{n-1}^+$ series from $n = 1$ to 12. These clusters form two cubes sharing a common corner, where each corner is occupied by either a cation or an anion.[26] Wakeham *et al*. suggest that these clusters exist at the IL/air interface with a thin layer of air surrounding them with the forces between ions preventing these clusters from evaporating. This situation for protic ILs is vastly different from the accepted surface structure of aprotic ILs where smaller clusters have been known to form in only a few ILs[27] but are not seen at the IL/vapour interface. However, the explanation of the geometry of the clusters as given by Ludwig does not indicate the degree of freedom that the cation molecules have in their orientation,[26] therefore the exact structure of the

[a] *Centre for NanoScale Science and Technology, Flinders University, SA, 5001, Australia. E-mail: gunther.andersson@flinders.edu.au*
[b] *School of Chemistry, The University of Sydney, NSW, 2006, Australia*

† Electronic supplementary information (ESI) available. See DOI: 10.1039/c2cp43035e

This journal is © the Owner Societies 2012

View Article Online

Published on 12 October 2012. Downloaded by Michigan State University on 19/01/2016 06:14:23.

surface of protic ILs is still relatively unknown. Wakeham *et al*. have shown that X-ray reflectivity measurements indicate that the surface of EtAN is covered with clusters similar to EAN and PAN, however there are no results to show what size or geometry these clusters would take. In fact, the lack of these clusters observed in other studies for diethanolammonium nitrate may be an indication that the extra hydroxyl functional group disrupts the hydrogen bonding network that stabilises these clusters. Therefore there is still a large degree of uncertainty in our understanding of the surface structure of these protic ILs owing to the unknown orientation of the cations in these clusters, and to the unknown orientation of the clusters themselves.

Metastable induced electron spectroscopy (MIES) is a technique ideally suited for investigating the free surface of ILs. In electron spectroscopy methods that use photons as probes (XPS, UPS), the photon penetrates well into the bulk of a sample. Hence the surface sensitivity of these methods is determined by the inelastic mean free path of the electron which is in the order of a few nanometres. MIES instead uses metastable helium atoms as the probes, which have a large cross section for de-excitation when colliding with an atom or a molecule. The excitation and electron emission process is thus sensitive to only the composition of the outermost layer of a sample. The excitation energy of MIES using metastable atoms is 19.8 eV while that of UPS is 21.2 eV when using the He I line. In the case of ionic liquids, the probing depth is usually at least as large as the distance between charge layers. Thus UPS can be used as a reference for identifying the molecular orbitals (MOs). A quantitative approach to the evaluation of MIES/UPS results can be achieved by calculating the MOs of the molecules constituting the target, which allows for accurate assignment of the individual MOs to their moiety of origin as described by Reinmöller *et al*.[28] Iwahashi *et al*. took this approach in their comprehensive investigation into the surface structure of the (aprotic) imidazolium-based IL series.[23] Although they did not take a quantitative approach to their evaluation, the calculation of MOs allows for a more precise approach to the data evaluation than would otherwise be possible.

MIES is complemented by neutral impact collision ion scattering spectroscopy (NICISS), which can be used to determine the concentration depth profiles of the elements up to a depth of around 20 nm and a resolution of a few Å close to the surface.[29] The three methods have not been combined before for analysing ILs and provide the opportunity for a quantitative and highly detailed investigation of the structure of protic IL surfaces. The aim of this study is to use MIES, UPS and NICISS in combination to determine the composition of the surface and the concentration depth profiles of the anion and the cation.

2. Experimental

a. Materials

The ILs were prepared by the dropwise addition of nitric acid (Sigma Aldrich) to the amine base (ethylamine, propylamine, ethanolamine, Fluka) in equimolar amounts. The solution was stirred over the course of the addition and kept below 15 °C. Water was removed from the product by rotary evaporation at 50 °C, then by purging with nitrogen while being heated to 110 °C overnight. Water content was then measured using Karl Fischer titration and found to be less than 0.1 wt% for all ILs after preparation. The structures of the ILs examined are shown in Fig. 1.

b. MIES/UPS

MIES/UPS experiments are performed in a UHV chamber with a base pressure of a few 10^{-10} mbar, although this pressure is not required for these measurements nor is it readily attainable due to the evaporation of trace amounts of water/gases in the IL. The probe source is a two stage cold cathode gas discharge from MFS (Clausthal-Zellerfeld, Germany) that simultaneously generates metastable helium (He* $^3S_1$) and UV photons (He I line). The emitted electrons are detected *via* a hemispherical Phoibos 100 energy analyser from SPECS (Berlin, Germany).

In a UPS experiment the target is irradiated by UV photons of energy E_{hv} (21.2 eV for the He I line) leading to the emission of photoelectrons from the target with a kinetic energy, E_{kin}, of

$$E_{kin} = E_{hv} - E_{bind} \quad (1)$$

where E_{bind} is the binding energy of the electron before excitation. In a UPS experiment the electron density in the surface near region is measured. The surface sensitivity of UPS is due to the limited escape depth of the emitted electrons (electron mean free path), which depends on the kinetic energy of the emitted electrons. For the range in kinetic energy considered in the evaluation of the spectra measured here, the electron mean free path is around 10 Å.[30] The kinetic energy of emitted electrons is measured with the hemispherical analyser. Knowing the excitation energy the binding energy of emitted electrons can be determined. MIES is similar to UPS, but uses metastable helium atoms (He*) as the electron excitation source. He* are de-excited at close proximity to the target *via* Auger de-excitation or resonant neutralisation with subsequent Auger neutralisation,[31] with the first process being dominant for the materials used in the present work. The majority of He* emitted from the source are in the $^3S_1$ state, which has an excitation energy of 19.8 eV. Exclusive sensitivity to the outermost layer is achieved due to the high cross-section for de-excitation of the He* which leads to the de-excitation process taking place

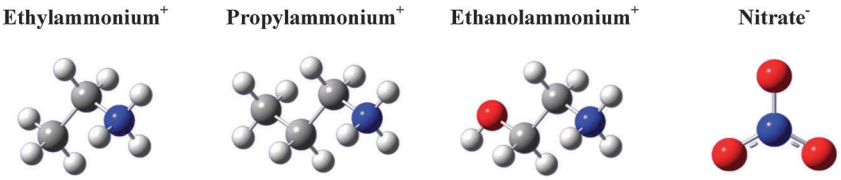

Fig. 1 Structure of the ions constituting the three ionic liquids, where grey is carbon, blue is nitrogen and red is oxygen.

View Article Online

Published on 12 October 2012. Downloaded by Michigan State University on 19/01/2016 06:14:23.

within a few Å of the surface.[33] The excitation energies used in MIES and UPS are appropriate for investigating MOs of the target. Multiple scans of each sample were taken, and no beam-induced changes were noticed in the spectra.

c. MO calculations

MO calculations were performed on an ion pair for each of the three ILs in this study with the aug-cc-pVTZ basis set (HF theory) using the Gaussian 09 package, with geometry optimisation performed. Original calculations were performed with the 6-31G** basis set with B3-LYP functional, however this resulted in the transfer of a proton from the cation ($R\text{-}NH_3^+$) to the anion (NO_3^-) resulting in two neutral molecules, an effect also seen by Lehmann *et al.*,[32] while the use of aug-cc-pVTZ basis set avoided this. Molecules were created and MOs were visualised using the GaussView 5.0 package.

d. Fitting the MIES/UPS spectra

The measured spectra are first fitted to the least amount of Gaussian functions (hereafter referred to simply as 'functions') required, such that their sum fits the measured spectra closely and accounts for all calculated MO energies. Each function is intended to represent an individual MO with a specific binding energy, but in some cases a single function represents a number of MOs with similar binding energies. The initial positions of the functions were based on the MO energies as calculated. After the fitting had been performed the resulting functions were then assigned to the cation or the anion based on which calculated MOs the functions best represented.

e. NICISS

In NICISS experiments the target is bombarded with a pulsed beam of He^+ ions with a primary energy of 3 keV.[31] The dose of the He^+ ions for this investigation was about 10^{10} ions per cm^2. The low dose is achieved by continuously refreshing the liquid surface to be investigated as described below. As a surface consists of a few 10^{14} atoms per cm^2, damage to the surface due to ion bombardment can be neglected. The measuring chamber is kept at a pressure of 10^{-5} mbar while the TOF tube and microchannel plates are kept at low 10^{-7} mbar.

The energy of the projectiles backscattered from the atoms in the target is determined by their time of flight (TOF) from the target to the detector. The projectiles lose energy during the backscattering process, and the energy transfer depends on the mass of the target atom. This first type of energy loss is used to identify the element from which a projectile is backscattered. Additionally, the projectiles experience a continuous energy loss on their trajectory through the bulk due to small angle scattering from and electronic excitations of the molecules constituting the target. This energy loss, known as the stopping power, is used to determine the depth of the atom from which the projectile is backscattered. In combination, these two types of energy losses are used to determine the concentration depth profiles of the elements. A typical NICIS spectrum consists (apart from the broad background of sputtered hydrogen) of energy loss spectra for each element in the sample. The shape of the spectrum of each element is determined by its concentration depth profile in the sample. The depth resolution of NICISS spectra is mainly influenced by small angle scattering of the projectile while on its trajectory through the bulk, which increases with trajectory length. Therefore in the top several Å of the surface this effect is minimal, leading to a depth resolution of only a few Å. The spectra are also influenced by the distribution of inelastic energy losses during the backscattering process and the straggling of the energy loss caused by low angle scattering and electronic excitations.[29] The inelastic energy loss during backscattering can be determined from the NICIS spectra of the respective elements in the gas phase. The energy loss straggling of low energy projectiles has been determined experimentally.[33] In order to determine the energy of a projectile backscattered from an element in the outermost layer of the sample, NICIS spectra of the elements in a low density gas jet are recorded. The spectrum of a gas jet consists almost entirely of projectiles backscattered from individual atoms, with no contribution from other energy-loss processes such as those due to the stopping power in a bulk sample. Therefore the measured spectrum of a gas jet consists of a series of peaks due to each element in the gas, each of which has a finite full-width-half-maximum (FWHM) mainly due to the distribution in inelastic energy losses during the collision process. The mean positions of these peaks are used to gauge the zero mark for the respective elements, and the FWHM (which is only a few Å for C, N, and O) determines the depth resolution near the surface.

NICISS is not able to detect surface topography or capillary waves at an incidence of the ion beam close to the surface normal, as depth information is obtained from the localised interaction of the projectiles with the constituents of the target. However, information about the local topography of a surface can be derived with the angle resolved ion scattering spectroscopy (ARISS) which is the angle resolved mode of NICISS.[34]

f. Experimental setup

For generating the liquid surface in the NICISS and MIES/UPS equipment the same type of setup has been used as described previously in detail[18,19] but will be briefly described here. A flat stainless steel disc is placed vertically inside a reservoir containing the IL, resulting in a liquid film of a few tenths of a millimetre in thickness covering the surface of the disc. The disc is then constantly rotated over the course of the experiment which allows for the constant replenishment of the liquid surface as well as aiding the evaporation of any dissolved water from the sample. This setup is designed such that it can be fully enclosed except for the presence of a small aperture in front of the disc. This minimises evaporation of the liquid while still allowing for measurement, however due to the negligible vapour pressure of ILs and the need to remove any water, this function was not used in these experiments. All ILs were held under vacuum (around 10^{-5} mbar) overnight prior to measurement in order to assist in the evaporation of water from the liquid.

3. Results and discussion

a. Outermost surface layer composition

Fig. 2 shows the UPS and MIES spectra of the three ILs investigated, together with the calculated energies of the occupied MOs.

 This journal is © the Owner Societies 2012

View Article Online

Published on 12 October 2012. Downloaded by Michigan State University on 19/01/2016 06:14:23.

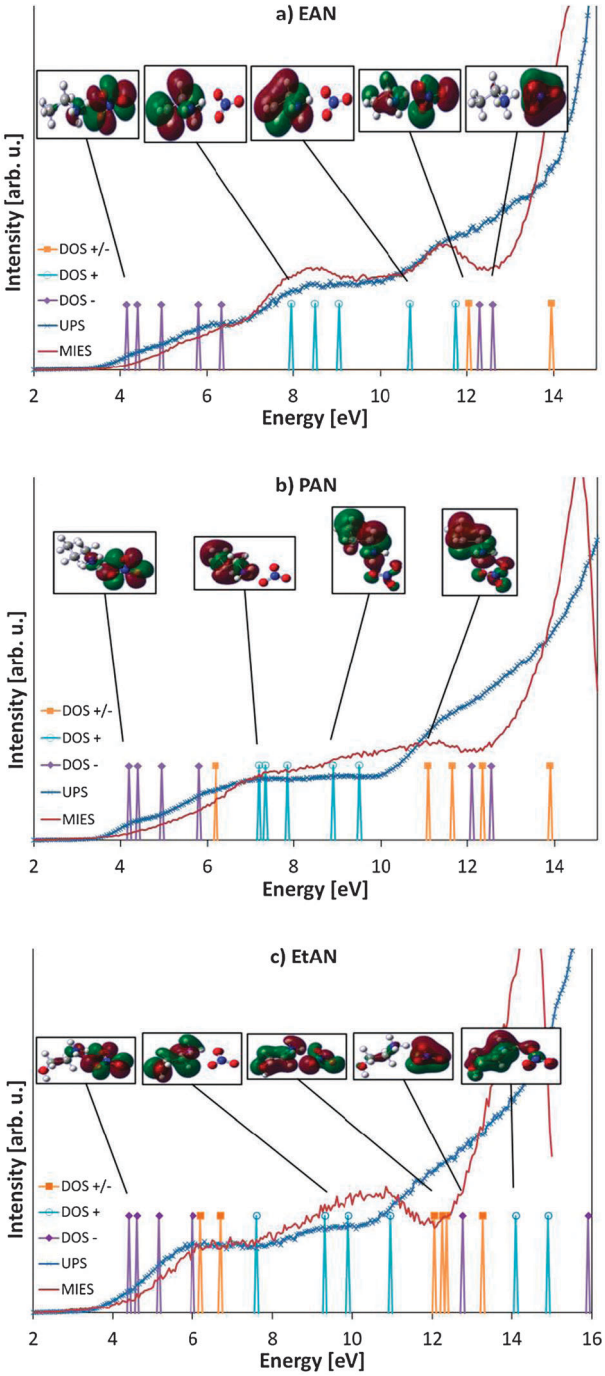

Fig. 2 MIE and UP spectra of the three ILs studied on binding energy scale along with MO eigenvalues. MOs were assigned to either the cation (+), the anion (−) or undefined (+/−) with the aid of MO visualisation. Samples of MO images are provided for the different assignments.

As discussed by Yoshimura *et al.*,[35] all calculated energies shown have been shifted in this experiment by −7 eV. Fig. 2 also shows images of typical MOs, which facilitates their assignment to either the cation or the anion. The highest occupied molecular orbital (HOMO) of the anion is at a considerably lower binding energy than the cation. In fact the majority of MOs for both the cation and the anion are well separated from each other at the high and low binding energy sides of the energy spectrum which allows for easier assignment of the experimental peaks to individual species. The spectra of calculated MOs also consist of a few orbitals with electron densities dispersed rather equally over both the cation and the anion that have been labelled as 'undefined'. These MOs sit at energies between the distinct anion and cation orbitals, therefore do not greatly hinder the assignment of MOs to the separate ions.

Fig. 3 shows the functions and the fit to the measured MIE spectra for the three ILs. The only variables between the MIE/UP spectra of a given IL were the intensities. Thus the change in

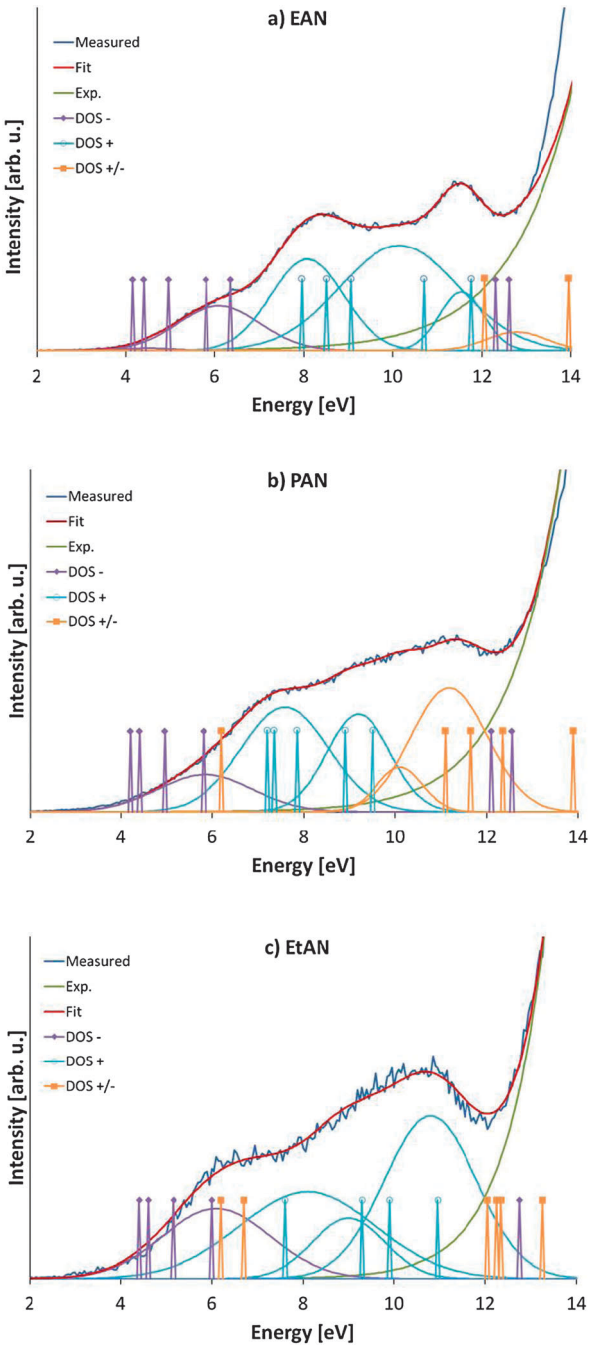

Fig. 3 MIE spectra of the three ILs along with the calculated MO eigenvalues and the Gaussian functions used to account for the MOs in the spectra.

View Article Online

Published on 12 October 2012. Downloaded by Michigan State University on 19/01/2016 06:14:23.

Table 1 Surface composition ratios, I_{norm}, derived from MIES and UPS, together with spectral data used in the determination

	Anion peaks used (eV)	Cation peaks used (eV)	R_{MIES}	R_{UPS}	I_{norm}
EAN	4.5, 6.0	8, 10.1, 11.53	5.66	3.61	1.57
PAN	4.3, 5.8	7.5, 9.2	4.31	1.79	2.40
EtAN	4.6, 6.1	8.2, 9.0, 10.8	4.14	1.76	2.35

intensity of the signals between MIES and UPS reflects differences in composition between the bulk and at the interface. As Iwahashi *et al.* point out in their MIES investigation of aprotic ILs, truly quantitative evaluation of MIES results is difficult to obtain due to unknown ionisation cross sections and the difficulty in removing the secondary electron background.[23] However, below we present a procedure which allows for a quantitative evaluation in the present work. The second step in peak assignment is to correlate the calculated MOs to the position of the fitted peaks. As can be seen in Fig. 2, the MOs owing to the anion are primarily observed at 4 to 6 eV, and those of the cation at 7.5 to 12 eV (see Table 1). This distinction in energy ranges for the anion and the cation allows for easier interpretation of the measured spectra.

Determining the surface composition with the anion and the cation for the ILs investigated can be achieved by comparing the ratios of the cation to the anion intensity found in the MIE spectra. However, because the cations are different for the three ILs investigated and because the cross sections of the interaction of the He* with the MOs are not known quantitatively, the intensity in the MIE spectra has to be normalised. Firstly the intensities for the cation and the anion in the MIE and UP spectra are summed up for each IL. As the MOs for the anion between 4 and 6 eV have exactly the same character and the MOs of the cation between 6.5 and 11 eV have very similar character (both pi and sigma character), the cross section for the interaction between the He* and the UV photons with the MOs of the cation and the anion should be very similar for the ILs investigated. A direct comparison of the MIES and UPS intensities, however, is not possible as the number of MOs in the cation is different for the investigated ILs. Comparison of the MIES intensities can be achieved by normalising the MIES intensities to the cation and the anion UPS intensities, as the probing depth of UPS is at least 15 to 20 Å and a good approximation to the bulk 1:1 composition. (This will be confirmed below with the concentration depth profiles determined by NICISS.) The MO intensities can thus be normalised by calculating

$$R_S = \left(\frac{\sum_n I_{cation,n}}{\sum_n I_{anion,n}} \right)_S \quad (2)$$

where R is the cation to anion ratio, S indicates either MIES or UPS, I_{cation} and I_{anion} is the intensity of an individual function owing to the cation or the anion, respectively, and n denotes the identity of the function being summed. The surface composition ratio or normalised intensity, I_{norm}, is then given by

$$I_{norm} = \frac{R_{MIES}}{R_{UPS}} \quad (3)$$

The larger I_{norm} is, the stronger is the presence of the specific cation at the surface. Table 1 shows the surface composition ratio for the three ILs examined, as well as which of the individual functions have been used. The results indicate that the cation is present in substantial excess over the anion at the outermost surface of all three ILs. While it is not surprising that PAN with its longer alkyl chain is present in greater excess than EAN, the large excess of EtAN and its similarity with PAN is unexpected.

b. Concentration depth profiles

Fig. 4 compares the elemental concentration depth profiles of the ILs (carbon, nitrogen and oxygen) normalised to their bulk values. In all cases the concentrations have reached their

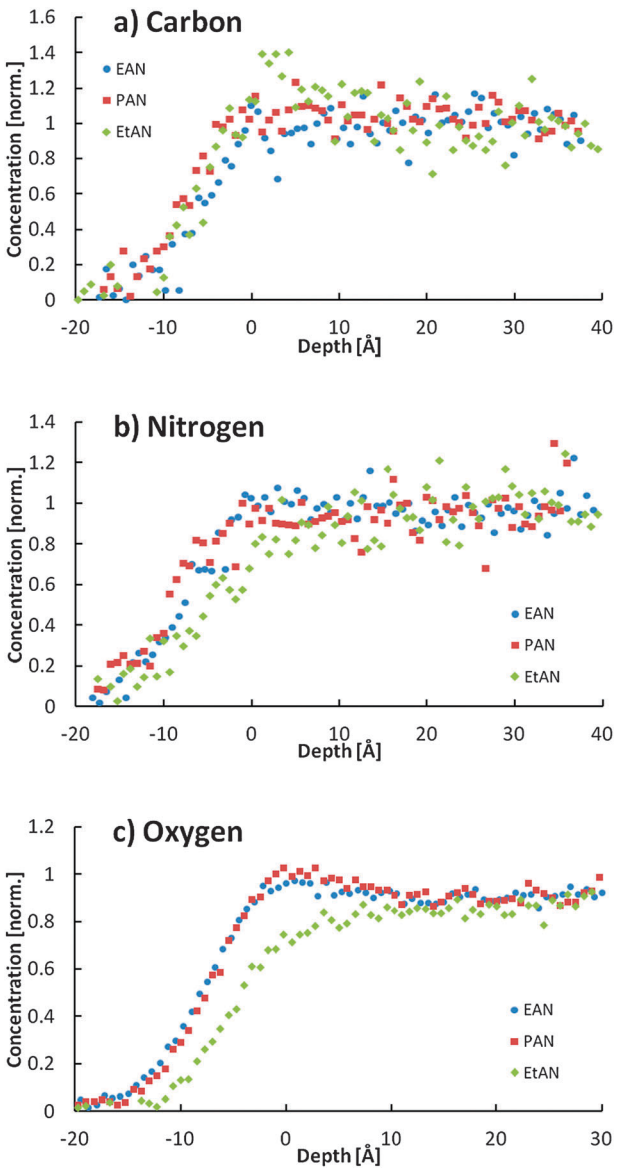

Fig. 4 Normalised elemental depth profiles of the three ILs investigated. The carbon profiles show a clear excess at the surface in EtAN that is not seen in EAN or PAN. Additionally, both nitrogen and oxygen are seen to be depleted at the surface of EtAN compared to EAN and PAN.

 This journal is © the Owner Societies 2012

View Article Online

Published on 12 October 2012. Downloaded by Michigan State University on 19/01/2016 06:14:23.

constant, bulk value by a depth of 10Å, validating the use of UPS to normalise MIES results above.

Fig. 4a shows that the carbon depth profile of PAN is shifted closer to the surface than the other ILs, indicating that cation chains are present at the outermost layer of the surface. The carbon profiles also show enrichment at the surface of EtAN that is not seen in the other two ILs, in the form of a 'spike' in concentration at zero depth for EtAN. This indicates that EtAN has a qualitatively different surface structure from PAN and EAN, with an excess of the cation alkyl chain at the surface. In contrast, the nitrogen and oxygen profiles show that they are both further away from the surface in EtAN than in EAN and PAN (as seen in Fig. 4b and c), while the nitrogen and oxygen profiles show little difference between EAN and PAN. As the nitrogen is present on both the cation and the anion (as is oxygen in EtAN), the increased nitrogen presence at the surface of EAN and PAN compared to EtAN could indicate either increased anion presence at the surface, or a decrease in the amount of cation with specific orientation of chains directed away from the bulk, the latter having the effect of moving the $-NH_3^+$ group closer to the outermost layer instead of sitting at the 'bottom' of the alkyl chains. Due to the MOs being delocalised over most of the molecule (anion or cation), it is not possible for MIES to accurately distinguish between the surface presence of the cation headgroup, $-NH_3^+$, the cation alkyl chain, or the hydroxyl group in the case of EtAN, hence this result is only seen directly by NICISS.

Further evaluation of these profiles is needed to understand the composition in the surface near region. Concentration depth profiles of different constituent moieties of the ILs (cation $-NH_3^+$, alkyl chain, and anion) can be calculated from linear combinations of the elemental depth profiles. *E.g.* carbon is present only in the cation, oxygen is only present on the anion for EAN and PAN and nitrogen is present on both the cation and the anion in fixed stoichiometries. The depth profiles of these moieties are shown in Fig. 5 for each IL investigated. The results show:

- The anion in EAN is closer to the surface compared to the other moieties (Fig. 5a) than in either PAN (Fig. 5b) or EtAN (Fig. 5c).
- Both EAN and PAN show rather homogenous distributions of all three moieties. Both the cation and the anion are present at the surface.
- EtAN is indeed qualitatively different, and shows a pronounced surface excess of the cation ethylene chain, accompanied by a shift of the cation head group and the anion below the surface. The shift away from the surface of oxygen also indicates that the hydroxyl groups are oriented beneath the ethylene chains, as has been seen previously.[36]

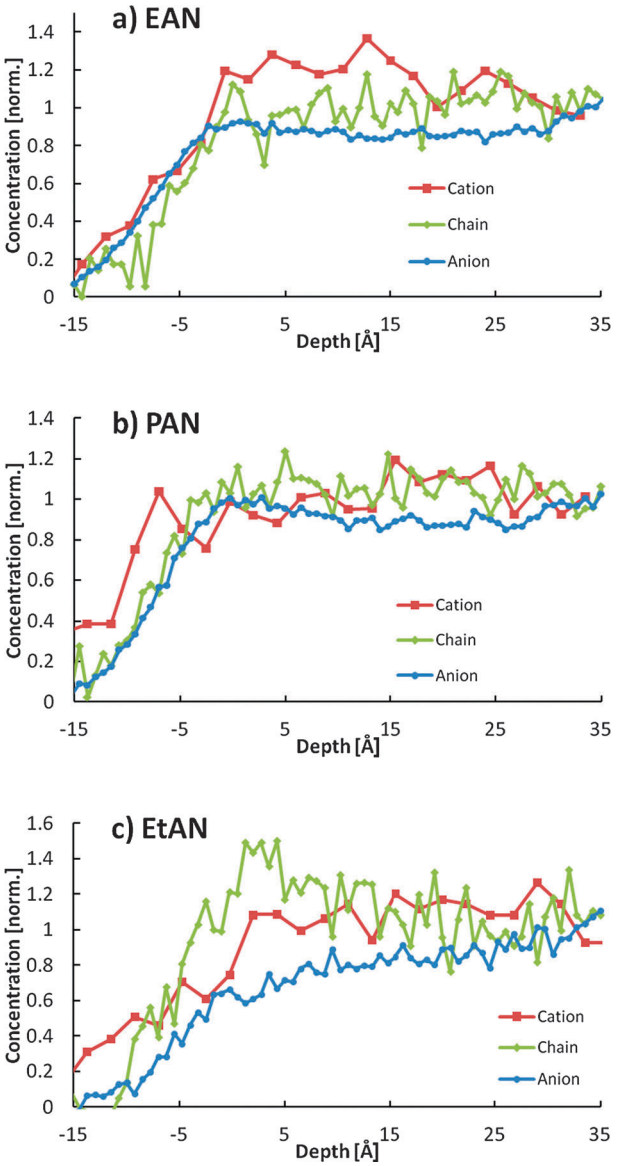

Fig. 5 Concentration depth profiles of the cationic ammonium, the anion and the cation alkyl chain in each of the three ILs investigated. The profiles indicate that while the surface of EAN is an homogenous distribution of the cation and the anion, PAN shows an increased orientation of the cation alkyl chains protruding from the surface, while EtAN shows a clear excess of the cation chain.

c. Surface structure of the ILs

These results reveal some unexpected similarities and differences between the surface structures of the three ILs studied. Overall, EtAN is the most straightforward to interpret. Although both cations and anions are present at the surface, the methylene carbons of the cations form an enriched and oriented layer, below which the ammonium cation, the hydroxyl group and the nitrate anion are buried and hence depleted from the outermost surface layer. This can be seen clearly in the NICISS results and is consistent with previous vibrational sum frequency spectroscopy results.[36] This cannot be concluded from the MIES/UPS results as the MOs of the cation are spread over the cation and in the present case do not allow to clearly distinguish between the alkyl chain and the nitrate group.

Both MIES/UPS and NICISS show that both the cation and the anion are present at the surface of EAN and PAN. MIES/UPS shows that propylammonium is more enriched over nitrate than ethylammonium in the surface layer. NICISS also shows discrimination between the cation and the anion throughout the interfacial region. For EAN the cation and anion profiles fall on top of each other while in PAN the cation

View Article Online

Published on 12 October 2012. Downloaded by Michigan State University on 19/01/2016 06:14:23.

and anion profiles are separated with the anion profile shifted away from the surface. The outermost surface layer is expected to contain alkyl chains oriented away from the bulk liquid, and this has been confirmed for EAN by vibrational sum frequency spectroscopy.[37] However, coverage of the outermost layer with the cation is stronger in the case of PAN than in EAN as shown by MIES/UPS. It is reasonable that the propyl group of PAN occupies a greater fraction of that surface than that of the ethyl on the grounds of both molecular volume and solvophobicity. Bulk neutron scattering studies have shown the existence of much more pronounced amphiphilic nanostructure in PAN than EAN.[38–40] X-ray reflectivity measurements also revealed layering of cations and anions (or polar and non-polar regions) in PAN and EAN, decaying over up to 30 Å into the bulk liquid. Quantitative analysis of scattering length density profiles showed that these correspond to only small compositional differences, and are thus not observed by NICISS.

4. Conclusion

The surface sensitive techniques NICISS and MIES/UPS were used to investigate the surface of the three protic ILs: EAN, PAN and EtAN. MO calculations were performed on ion pairs of the three ILs studied in order to perform a semi-quantitative evaluation of the electron spectroscopy data. MIES/UPS results show that the cation is enriched over the anion in the outermost surface layer of all three ILs examined, but that both ions are present. The degree of cation enrichment is smaller for EAN than EtAN and PAN, which had similar surface compositions. NICISS depth profiles reveal further information on the surface structure. EtAN shows an excess of carbon (owing to the cation alkyl chain) in the top several Å which is not seen in PAN or EAN. This is followed by a shifting away from the surface of nitrogen and oxygen as found in the concentration depth profiles, indicating that the carbon atoms in the cation chain are sitting above the centre of the cation and hydroxyl group in the surface. Conversely, the carbon profile being shifted toward the surface in the case of PAN indicates an orientation of the cation with the chains protruding straight out of the surface, pointing towards the vapour phase. The results are consistent with either clusters at the surface or a simple liquid interface with a sharp density profile at the interface. In both cases the description of the ion positions and orientations is the same for the outermost layer. Additionally, while the amount of cation seen at the outermost layer is different between the ILs it is important to note that the anion is always present, *i.e.* there is no exclusive selection of ions at the surface. In either regard, the results provide further evidence for the high extent of property tailoring in protic ILs.

Acknowledgements

This work has been supported by grants of the Australian Research Council (LE0989068 and DP0986194) and a University of Sydney Bridging Support Grant. The authors want to thank Rob Atkin from Newcastle University for supplying some of the ionic liquids and for fruitful discussions. The authors also want to thank Greg Metha and Jason Alvino from Adelaide University for their support of the MO calculations.

References

1 S. Chowdhury, R. S. Mohan and J. L. Scott, *Tetrahedron*, 2007, **63**, 2363–2389.
2 C. Pinilla, M. G. Del Pópolo, R. M. Lynden-Bell and J. Kohanoff, *J. Phys. Chem. B*, 2005, **109**, 17922–17927.
3 D. Wei, *Int. J. Mol. Sci.*, 2010, **11**, 1103–1113.
4 R. D. Rogers and K. R. Seddon, *Ionic Liquids IIIB Fundamentals, Progress, Challenges and Opportunities: Transformations and Processes*, Oxford University Press, 2005.
5 T. Itoh, E. Akasaki, K. Kudo and S. Shirakami, *Chem. Lett.*, 2001, **30**, 262–263.
6 P. Scovazzo, *J. Membr. Sci.*, 2009, **343**, 199–211.
7 W. Ren and A. M. Scurto, *AIChE J.*, 2009, **55**, 486–493.
8 S. Rivera-Rubero and S. Baldelli, *J. Phys. Chem. B*, 2006, **110**, 15499–15505.
9 C. S. Santos and S. Baldelli, *J. Phys. Chem. B*, 2007, **111**, 4715–4723.
10 Y. Jeon, J. Sung, W. Bu, D. Vaknin, Y. Ouchi and D. Kim, *J. Phys. Chem. C*, 2008, **112**, 19649–19654.
11 E. Sloutskin, B. M. Ocko, L. Tamam, I. Kuzmenko, T. Gog and M. Deutsch, *J. Am. Chem. Soc.*, 2005, **127**, 7796–7804.
12 Y. Lauw, M. D. Horne, T. Rodopoulos, N. A. S. Webster, B. Minofar and A. Nelson, *Phys. Chem. Chem. Phys.*, 2009, **11**, 11507–11514.
13 D. Wakeham, A. Nelson, G. G. Warr and R. Atkin, *Phys. Chem. Chem. Phys.*, 2011, **13**, 20828–20835.
14 G. Law, P. R. Watson, A. J. Carmichael and K. R. Seddon, *Phys. Chem. Chem. Phys.*, 2001, **3**, 2879–2885.
15 V. Lockett, R. Sedev, S. Harmer, J. Ralston, M. Horne and T. Rodopoulos, *Phys. Chem. Chem. Phys.*, 2010, **12**, 13816–13827.
16 V. Lockett, R. Sedev, C. Bassell and J. Ralston, *Phys. Chem. Chem. Phys.*, 2008, **10**, 1330–1335.
17 C. Kolbeck, T. Cremer, K. R. J. Lovelock, N. Paape, P. S. Schulz, P. Wasserscheid, F. Maier and H. P. Steinrück, *J. Phys. Chem. B*, 2009, **113**, 8682–8688.
18 C. Ridings, V. Lockett and G. Andersson, *Phys. Chem. Chem. Phys.*, 2011, **13**, 21301–21307.
19 C. Ridings, V. Lockett and G. Andersson, *Phys. Chem. Chem. Phys.*, 2011, **13**, 17177–17184.
20 T. Hammer, M. Reichelt and H. Morgner, *Phys. Chem. Chem. Phys.*, 2010, **12**, 11070–11080.
21 O. Höfft, S. Bahr, M. Himmerlich, S. Krischok, J. A. Schaefer and V. Kempter, *Langmuir*, 2006, **22**, 7120–7123.
22 S. Krischok, M. Eremtchenko, M. Himmerlich, P. Lorenz, J. Uhlig, A. Neumann, R. Öttking, W. J. D. Beenken, O. Höfft, S. Bahr, V. Kempter and J. A. Schaefer, *J. Phys. Chem. B*, 2007, **111**, 4801–4806.
23 T. Iwahashi, T. Nishi, H. Yamane, T. Miyamae, K. Kanai, K. Seki, D. Kim and Y. Ouchi, *J. Phys. Chem. C*, 2009, **113**, 19237–19243.
24 A. Ray, *Nature*, 1971, **231**, 313–315.
25 D. F. Kennedy and C. J. Drummond, *J. Phys. Chem. B*, 2009, **113**, 5690–5693.
26 R. Ludwig, *J. Phys. Chem. B*, 2009, **113**, 15419–15422.
27 R. Bini, O. Bortolini, C. Chiappe, D. Pieraccini and T. Siciliano, *J. Phys. Chem. B*, 2006, **111**, 598–604.
28 M. Reinmoller, A. Ulbrich, T. Ikari, J. Preiss, O. Hofft, F. Endres, S. Krischok and W. J. D. Beenken, *Phys. Chem. Chem. Phys.*, 2011.
29 G. Andersson and H. Morgner, *Surf. Sci.*, 1998, **405**, 138–151.
30 M. P. Seah and W. A. Dench, *Surf. Interface Anal.*, 1979, **1**, 2–11.
31 H. Morgner, in *Advances In Atomic, Molecular and Optical Physics*, ed. B. Benjamin and W. Herbert, Academic Press, 2000, vol. 42, pp. 387–488.
32 S. B. C. Lehmann, M. Roatsch, M. Schoppke and B. Kirchner, *Phys. Chem. Chem. Phys.*, 2010, **12**, 7473–7486.
33 G. Andersson, *Phys. Rev. A*, 2007, **75**, 032901.

 This journal is © the Owner Societies 2012

View Article Online

34 G. Andersson, T. Krebs and H. Morgner, *Phys. Chem. Chem. Phys.*, 2005, **7**, 2948–2954.
35 D. Yoshimura, T. Yokoyama, T. Nishi, H. Ishii, R. Ozawa, H. Hamaguchi and K. Seki, *J. Electron Spectrosc. Relat. Phenom.*, 2005, **144–147**, 319–322.
36 D. Wakeham, P. Niga, C. Ridings, G. Andersson, A. Nelson, G. G. Warr, S. Baldelli, M. W. Rutland and R. Atkin, *Phys. Chem. Chem. Phys.*, 2012, **14**, 5106–5114.
37 P. Niga, D. Wakeham, A. Nelson, G. G. Warr, M. Rutland and R. Atkin, *Langmuir*, 2010, **26**, 8282–8288.
38 R. Hayes, S. Imberti, G. G. Warr and R. Atkin, *Phys. Chem. Chem. Phys.*, 2011, **13**, 13544–13551.
39 R. Hayes, G. G. Warr and R. Atkin, *Phys. Chem. Chem. Phys.*, 2010, **12**, 1709–1723.
40 R. Atkin and G. G. Warr, *J. Phys. Chem. B*, 2008, **112**, 4164–4166.

Published on 12 October 2012. Downloaded by Michigan State University on 19/01/2016 06:14:23.